C. R. Chimie 15 (2012) 298–310

Contents lists available at SciVerse ScienceDirect

Comptes Rendus Chimie

www.sciencedirect.com

Full paper/Mémoire

Synthesis, characterization, magnetic, thermal and electrochemical studies of oxidovanadium (IV) picolyl hydrazones as functional catechol oxidase models

Amina A. El-Taras, Ibrahim M. EL-Mehasseb, Abd El-Motaleb M. Ramadan *

Chemistry Department, Faculty of Science, Kafr El-Sheikh University, 33516 Kafr-El-Sheikh, Egypt

ARTICLE INFO

Article history:
Received 6 July 2011
Accepted after revision 15 November 2011
Available online 17 January 2012

Keywords:
Synthesis
Characterization
Magnetic
Thermal
Oxidovanadium (IV)
Hydrazones
Catechol oxidase models

ABSTRACT

The picolyl hydrazone ligands derived from picolonic acid hydrazide and α-pyridyle ketone (L^1, L^2 and L^3), α-acetyl thiophene (L^4), α-formyl or α-acetyl phenol (L^5 and L^6 respectively) and 2-hydroxy-1-naphthaldehyde (L^7) react with equimolecular amount of vanadyl sulfate in refluxing methanol to yield oxidovanadium (IV) complexes. The structure of the obtained ligands and their oxidovanadium (IV) complexes were characterized by various physicochemical techniques, viz. elemental analysis, molar conductance, magnetic susceptibility measurements, thermal analysis (TGA & DTG), IR, electronic absorption and ESR spectral studies. Cyclic voltammeteric behavior of the complexes has also been discussed. Five-coordinate square-pyramidal structure was proposed for all complexes. A monomeric nature was reported for complexes *(2)*, *(3)*, *(6)*, and *(7)*, while dimeric structures were suggested for complexes *(1)*, *(4)* and *(5)*. The ability of the complexes to catalyze the aerobic oxidation of catechol to the light absorbing *o*-quinone has been investigated. The results obtained show that all complexes catalyze this oxidation reaction and large variations in the rate were observed. Electrochemical data for most complexes show that there is a linear relationship between their ability to oxidize catechole and their $E_{1/2}$ potentials. The most effective catalysts were those complexes which exhibited $E_{1/2}$ values approached to the E° value of the natural tyrosinase enzyme isolated from mushroom, while those that largely deviated from that potential exhibited lower oxidase catalytic activity. The probable mechanistic implications of the catalytic oxidation reactions are discussed.

1. Introduction

In recent years, vanadium chemistry has attracted attention due to its interesting structural features and biological relevance [1–3]. Applications of vanadium compounds in medicine have focused their activity, in vitro and in vivo, in the treatment, of insulin deficiency type I diabetes, and insulin tolerance, type 2 diabetes. Besides the insulin-like activity of oxidovanadium (V) and oxidovanadium (IV) compounds [4,5], its presence in vanadium dependent haloperoxidases has particularly stimulated the search for structural and functional models. Vanadium haloperoxidases are enzymes capable of oxidizing halide by hydrogen peroxide to hypohalous acids HOX [6,7].

The current catalytic interest in the high-valent vanadium complexes arises from the presence of vanadium in several metalloenzymes [8–10]. These complexes have been considered as new versatile catalytic reagents for a wide range of oxidation reactions, like oxidation of olefins and allylic alcohols [11–14], benzene/alkylaromatic compounds [15,16], sulfides [17–19] and alcohols [20–22]. These catalytic reactions have been performed

* Corresponding author.
E-mail address: ramadanss@hotmail.com (A.E.M. Ramadan).

1631-0748/$ – see front matter © 2011 Académie des sciences. Published by Elsevier Masson SAS. All rights reserved.
doi:10.1016/j.crci.2011.11.009

chiefly in homogeneous conditions. The homogeneous system has the advantage of the high rate of catalytic reaction, whereas some disadvantages include the difficulty in separation of the reaction product from the catalyst.

In vanadium chemistry, the VO^{2+} and VO^{3+} motifs have received considerable attention probably due to their involvement in many vanadium-dependent enzymes, viz., nitrogenases [23], haloperoxidases [24,25], etc. In most vanadium oxidase models the active site contains these two motifs are coordinated by oxygen-nitrogen donor atoms. The strong affinity of these two motifs towards *O*-, *N*-donor ligand is probably due to their hard acidic nature and selective stabilization of these two motifs depends upon the basicity of donor atoms. Hydrazone ligands derived from the condensation of acid hydrazides with, α-pyridyle ketone, and aromatic 2-hydroxy carbonyl compounds, are important tridentate *O*-, *N*-donor ligands containing two intermediate basic groups viz., phenolic, amide groups (which bind through their enol forms) and one neutral imine moiety. These ligands are of particular interest because they provide coordination environments which efficiently stabilize different oxidation states of vanadium, while still providing active sites capable of binding other molecules [26].

However, to the best of our knowledge, the mononuclear oxidovanadium (IV) complexes derived from the hydrazone ligands exhibiting catecholase-like activity have not been reported. Herein we report the synthesis, and structural characterization of some new oxidovanadium (IV) hydrazones (Schemes 1 and 2), subsequently investigated as functional models of the catechol oxidase enzyme.

2. Experimental

2.1. Materials

All chemical used were of analytical grade. The reported hydrazone ligands were prepared according to the method described elsewhere [27]. Catechol was purified by recrystalization twice from diethyl ether.

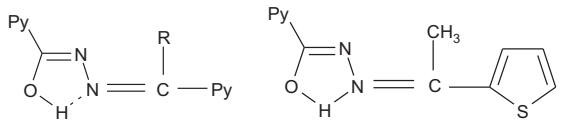

L^1, R=H; L^2, R=CH_3; L^3, R=Ph L^4

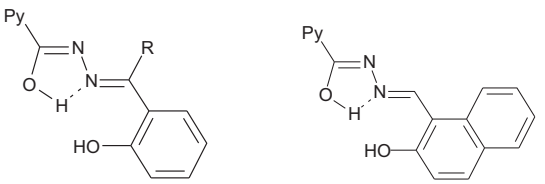

L^5, R=H; L^6, R=CH_3 L^7

Scheme 1.

2.2. Physical measurements

The i.r. spectra were recorded using KBr disks in the 4000–200 cm^{-1} range on a Unicam SP200 spectrophotometer. The electronic absorption spectra were obtained in DMF solution with a Shimadzu UV-240 spectrophotometer. Magnetic moments were measured by Gouy's method at room temperature. ESR measurements of the polycrystalline samples at room temperature were made on a Varian E9 X-band spectrometer using a quartz Dewar vessel. All spectra were calibrated with DPPH ($g = 2.0027$). The specific conductance of the complexes was measured using freshly prepared 10^{-3} M solutions in electrochemically pure MeOH or DMF at room temperature, using an YSI Model 32 conductance meter. The thermogravimetric measurements were performed using a Shimadzu TG 50-Thermogravimetric analyzer in the 25–800 °C range and under an N_2 atmosphere. Elemental analyses (C, H, and N) were carried out at the Micro analytical Unit of Cairo University.

2.3. Electrochemical measurements

Cyclic voltammetric measurements were performed by a computerized Electrochemical Trace Analyzer Model 273A-PAR (Princeton Applied Research, Oak Ridge, TN, USA) controlled via 270/250 PAR software was used for the cyclic voltammetry measurements. The electrode assembly (Model 303A-PAR) incorporating of a micro-electrolysis cell of a three electrode system comprising of a hanging mercury drop electrode as a working electrode (area: 0.026 cm^{-1}), an $Ag/AgCl/KCl_s$ reference electrode and a platinum wire counter electrode, was used. Stirring of the solution in the micro-electrolysis cell was performed using a magnetic stirrer (305-PAR) to provide the convective transport during the preconcentration step. The whole measurements were automated and controlled through the programming capacity of the apparatus. The supporting electrolyte used was 0.1 M *n*-Bu_4NClO_4. The solvents used were sufficiently pure and the concentration of the complexes was 0.001 M.

2.4. Synthesis of the oxidovanadium (IV) hydrazones

A hot methanolic solution (50 cm^3) of the vanadyl sulfate salt (0.01 M) was added to a boiling solution of the hydrazone ligand (0.01 M) in a pure dry methanol (50 cm^3) with constant stirring and the reaction mixture was refluxed for 2 h. The reaction mixture was then allowed to stand at room temperature overnight, whereby a microcrystalline product was formed. The resulting colored precipitates were filtered off, washed several times with cold methanol, ether and finally dried in evacuated desiccators over CaO (yield 60–75%).

2.5. Catechol oxidase biomimetic catalytic activity

The catechol oxidase biomimetic catalytic activity of the synthesized oxidovanadium (IV) complexes under atmospheric air were followed spechtrophotometerically by monitoring the increase in the *o*-quinone absorbance at 400 nm. DMF solution of the oxidovanadium (IV) complexes 1 ml (0.001 M) and 1 cm^3 solution of 4-*tert*-butyl catechol in

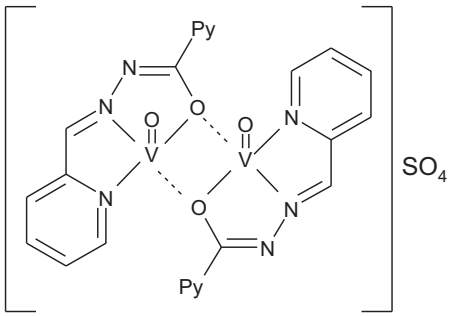

(1)

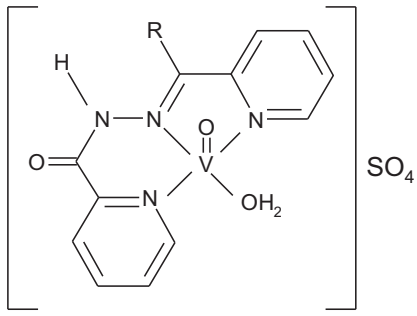

For *(2)*, R = CH_3, For *(3)*, R=Ph

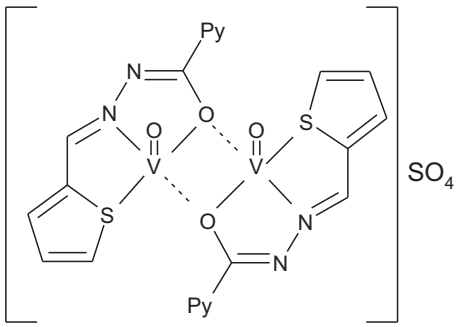

(4)

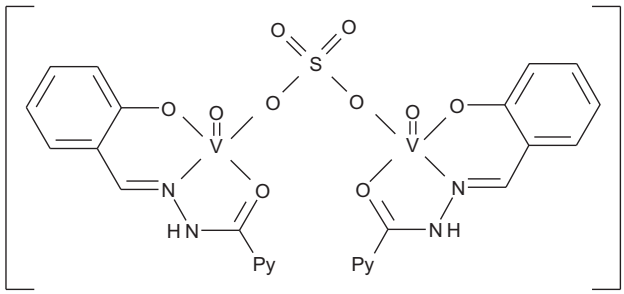

(5)

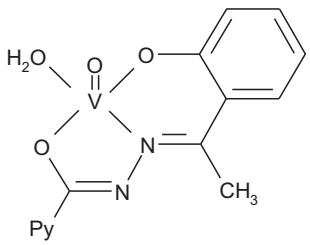

(6)

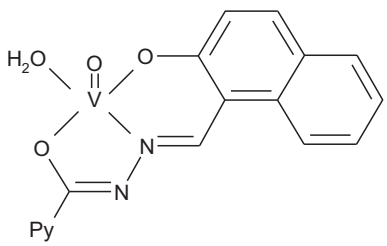

(7)

Scheme 2.

DMF (0.1 M) were combined in a quartz cell at room temperature in presence of 1 cm^3 of Et_3N (0.1 M). The absorbance changes at 400 nm were recorded at different time intervals. Formation of *o*-quinone was also detected by thin layer chromatography technique using authentic sample of *o*-quinone.

3. Results and discussion

3.1. General

The picolyl hydrazones ligands used in this study are derived from Schiff base condensation in a 1:1 molar ratio

Table 1
Molecular formulae, elemental analyses, and physical properties of oxidovanadium (IV) hydrazones.

Complex	Color	Λ (Ω^{-1} cm^2 mol^{-1})	Found (cacld.) %C	%H	%N	%M
(1) $[(VOL^1)_2]SO_4$ $4H_2O$	Dark brown	97.89	39.82 (39.99)	3.75 (3.61)	15.44 (15.56)	14.03 (14.16)
(2) $[(VOL^2)$ $H_2O]$ SO_4 H_2O	Brown	60.41	36.29 (36.87)	4.13 (3.78)	12.80 (13.24)	12.54 (12.05)
(3) $[VOL^3$ $H_2O]$ SO_4 H_2O	Pale green	61.80	44.33 (44.53)	3.87 (3.71)	11.35 (11.55)	09.97 (10.51)
(4) $[(VOL^4)_2]$ SO_4 H_2O	Green	150.16	38.68 (38.89)	3.89 (3.24)	10.68 (11.35)	13.25 (13.77)
(5) $[(VOL^5)_2$ $SO_4]$ H_2O	Dark red	149.89	44.59 (44.79)	2.87 (3.15)	11.82 (12.06)	14.68 (14.64)
(6) $[VOL^6$ $H_2O]$ H_2O	Yellowish brown	20.14	49.49(49.37)	4.53 (4.41)	12.55 (12.35)	14.25 (14.98)
(7) $[VOL_7$ $H_2O]$	Yellowish red	43.96	56.23 (56.93)	3.45 (3.63)	11.60 (11.73)	14.32 (14.23)

of the picolonic acid hydrazide with α-pyridyle ketone (L^1, L^2 and L^3), α-acetyl thiophene (L^4), α-formyl or α-acetyl phenol (L^5 and L^6, respectively) in addition to 2-hydroxy-1-naphthaldehyde (L^7) as shown in Scheme 1. This ligand system can act as a tridentate ligand, allowing coordination in its neutral or mono- and dianionic form due to the presence of the amide functionality which permits a keto-enol equilibrium.

Interaction of vanadyl sulfate with the title ligands in equimolar ratio in methanolic solution produces the tetravalent five-coordinate oxidovanadium (IV) complexes *(1-7)* in an appreciable yield. Chemical analysis and some physical properties of the pure isolated oxidovanadium (IV) complexes are listed in Table 1. The analytical results demonstrate that all the complexes have (1:1) metal:ligand ratio. The pure solid chelates are various shades of brown, except for complex *(3)* and *(4)* which are various shades of green. The pure microcrystalline complexes are freely soluble in DMF partially soluble in methanol (with exception of complex *(5)*, which is freely soluble) and completely insoluble in water. The monomeric complexes 2 and 3 have electrical molar conductivities approaching 1:1 electrolytic behavior. Complexes *(1)* and *(4)* behave as 1:1 electrolytes with molar conductance values of 147.63 – 150.16 Ω^{-1} cm^2 mol^{-1}, suggesting that in the poorly coordinating methanol solution the sulfate group is not bound directly to the central oxidovanadium (IV) ion in the five-coordinate dimeric structure. Based on the proposed formulae (Scheme 2), it is expected that, the oxidovanadium (IV) centers can achieve their coordination saturation by the binding to the polar groups (e.g., O) of the neighboring ligand molecule. As indicated by the magnetic studies, there seem to be an exchange interaction between the metal ions. These results confirm the dimeric structure of the complexes *(1)* and *(4)* in the solid state. On the other hand, in DMF solution these complexes exhibit molar conductance values (147.63 – 150.16 Ω^{-1} cm^2 mol^{-1}) characteristic to 1:2 electrolytic behavior. Hence, we propose that in the highly polar DMF solution the dimeric structure is broken down and the oxidovanadium (IV) centers can achieve the 5- or 6-coordinated structures by the binding to solvent molecules. Concerning complex *(5)*, the low electrical conductance in the methanolic solution indicates its non-electrolytic nature, while in DMF solution it behaves as 1:2 electrolyte. However, the non-electrolytic nature of the complex *(5)* in the poorly coordinating methanol suggests that the sulfate group is participating in the coordination sphere as a bridge in a dimeric structure (Scheme 2). This conclusion is further supported by the results of i.r. spectra and the magnetic moment measurements. Accordingly, we suggest that a solvolysis reaction takes place in the highly polar DMF solution as shown in the following interactions:

$$\left[(VOL^n)_2\right]SO_4 + 2DMF \rightleftharpoons 2\left[VOL^nDMF\right]^+ + {SO_4}^{2-}, n = 1 \text{ or } 4$$

$$\left[\left(VOL^5\right)_2SO_4\right] + 2DMF \rightleftharpoons 2\left[VOL^5\,DMF\right]^+ + {SO_4}^{2-}$$

For complexes *(6)* and *(7)* the molar conductivities obtained in DMF solution demonstrate that these complexes are non-electrolytes with Λ_M values lying in the 20.14–43.96 Ω^{-1} cm^2 mol^{-1} range.

3.2. Mode of bonding

Important vibration bands of the free ligands and their oxidovanadium complexes, which are useful for determining the mode of coordination of the ligands, are given in Table 2. The free picolyl hydrazones exhibit bands in the region 3412–3541, 3189–3338 and 1664–1699 cm^{-1} assigned to the intramolecular H-bonding vibration (O–H···N), OH, NH and C=O stretches, respectively [27]. These bands disappear on complexation, indicating the transformation of carbonyl moiety to enolic moiety and consequence replacement of the enolic hydrogen by the oxidovanadium (IV) ion (complexes *(1)*, *(4)*, *(6)* and *(7)*). A new band appearing in the 1247–1289 cm^{-1} region in the spectra of complexes *(1)*, *(4)*, *(6)* and *(7)*) was assigned to the υ(C–O) of the enolate mode [28,29]. The spectra of complexes 2 and 3 display no changes of υ(C=O) and υ(N–H) bands upon complex formation. This denotes that coordination of the tridentate ligand L^2 and L^3 may take place through the two pyridine nitrogens and the nitrogen atom of the Schiff base linkage (Scheme 2). As regards complex *(5)* the υ(N–H) band is almost unaffected by complex formation, whereas the υ(C=O) absorption band is shifted by 24 cm^{-1} to higher wave numbers indicating the bonding of the ligand to the metal ion through the carbonyl oxygen. For complexes *(6)* and *(7)* the coordination may take place through both the deprotonated phenolate and enolate oxygens, in addition to the nitrogen atom of the azomethine linkage. The band appearing at 1334–1343 cm^{-1} for complexes (5) and (6) was assigned to υ(ph–O) [30]. In the spectra of the reported ligands the characteristic bands of the pyridine ring are observed at 750–766 cm^{-1}. When the spectra of the complexes *(4)*, *(5)*, *(6)* and *(7)* were compared to the free ligands, changes

Table 2
The characteristic i.r. frequencies (cm^{-1}) of oxidovanadium (IV) hydrazones.

Compound	υ(OH)	υ(NH)	υ(C=O)	υ(C=N)	δ(py)	υ(M – O)	υ(M – N)
L^1	3427	3293	1694	1576	761	–	–
(1)	–	–	–	1613	768	554	459
L^2	3541	3311	1699	1572	745	–	–
(2)	–	–	–	1598	768	553	462
L^3	3440	3301	1688	1632	761	–	–
(3)	–	3300	1687	1597	772	–	459
L^4	3412	3320	1695	1623	766	–	–
(4)	–	–	–	1597	766	558	458
L^5	3539	3266	1678	1614	750	–	–
(5)	–	3265	1734	1602	753	515	445
L^6	3649	3337	1696	1599	744	–	–
(6)	–	3338	1697	1598	755	535	467
L^7	3484	3189	1664	1580	739	–	–
(7)	3437	–	–	1604	752	512	440

Complex details are as listed in Table 1.

were not observed in the vibrations of the pyridine ring, indicating that the nitrogen atom of the pyridine ring does not take part in coordination. On the other hand for complexes (1), (2) and (3), the characteristic in-plan ring deformation bands of the pyridine ring shift to higher energy revealing coordination of the pyridine ring N-atom [31]. Coordination of the nitrogen atoms to $V{=}O^{2+}$ ion is further supported by the appearance of new absorption band at 440–467 cm^{-1} range which are assigned to the υ(N–M) [32]. Thiophene stretching is observed at 775 cm^{-1} in the free ligand (L^4). In complex *(4)* this band appears at lower frequency at 765 cm^{-1} confirming the involvement of the thiophene sulfur in complex formation [33].

For all complexes the characteristic absorption band of $\upsilon(V{=}O^{2+})$ was observed in the 960–980 cm^{-1} region. The υ(V–O) stretching mode which originated from interaction of the tetravalent cation (VO^{2+}) with carbonyl, enolate or phenolate oxygen was observed in the lower frequency region 512–558 cm^{-1} in the spectra of the reported complexes [32].

For complexes *(1)*, *(4)* and *(5)* the medium strong bands present in the range 3450–3550 cm^{-1}, assignable to υ(OH), clearly confirm the presence of lattice water. Since vibrational modes such as wagging, twisting and rocking activated by coordination to the metal have not been found in the expected ranges, it appears that coordinated water is not present. These results are consistent with the thermogravimetric studies, using TG and DTG techniques; in fact this water is lost in the 70–125 °C range.

In the spectra of complexes *(2)*, *(3)*, *(6)* and *(7)* the characteristic absorption of the coordinated water is observed between 900–930, 790–800 and 660–675 cm^{-1}, including the wagging, twisting and rocking vibrations [32]. This finding is further supported by the results of thermal analysis.

For complexes *(1)* and *(4)* a dimeric structure is expected, where interaction of oxidovanadium (IV) ion with the free electron pairs of the oxygen atoms of a neighboring complex molecules confers coordination saturation in the five coordinate square-pyramidal conformation. This mode of interaction has been identified in analogues oxidovanadium (IV) hydrazones [34]. Complexes *(1)* and *(4)* have a new band in the region 833–845 cm^{-1} indicating V–O–V bridge vibrations [35]. The formation of V–O–V ridge is further supported from the magnetic studies results.

The spectra of complexes *(1)*, *(2)*, *(3)* and *(4)* show strong band at about 730–745 cm^{-1} and weak band at about 1250–1264 cm^{-1}, which indicates the ionic character of SO_4 [32]. The appearance of new bands at 941(υ_1), 1155(υ_2) and 657(υ_3) cm^{-1} in the spectrum of complex *(5)* suggests the bidentate bridging nature of the sulfato group of C_{2v} symmetry [32].

3.3. Electronic absorption spectra

The electronic absorption spectra of the title ligands and their oxidovanadium (IV) complexes were recorded in solution and the results obtained are given in Table 3. In the low energy region the spectra of all complexes display three low-intensity bands, the second of which is present as a shoulder in the 16,949–18,348 cm^{-1} range. These bands can be assigned to $^2B_{2g} \rightarrow {}^2E_{2g}$, $^2B_{2g} \rightarrow {}^2B_{1g}$ and $^2B_{2g} \rightarrow {}^2A_{1g}$ transitions respectively [36]. According to Ballhausen and others [37,38], these energy absorption bands are assigned to the ligand field transitions: $d_{xy} \rightarrow (d_{xz}, d_{yz})$, $d_{xy} \rightarrow d_x{}^2{-}_y{}^2$ and $d_{xy} \rightarrow d_Z{}^2$ corresponding to $b_2 \rightarrow e^*$ (υ_1), $b_2 \rightarrow b_1{}^*$ (υ_2) and $b_2 \rightarrow a_1{}^*$ (υ_3) transitions respectively [39]. These spectral characteristics suggest that the synthesized oxidovanadium (IV) hydrazones are five-coordinate, square-pyramidal structure [40]. Furthermore, in the high energy region, the strong absorption band in the 33,222–29,239 cm^{-1} range of the free ligands is assignable to the $n \rightarrow \pi^*$ transition originating from the azomethine linkage of the Schiff-base moiety [41]. The position and intensity of this band show dependence on the nature of the substituents within the carbonyl imine moiety of the ligands. The presence of the electron- donating group (CH_3) in L^2 shifts the $n \rightarrow \pi^*$ transition to the higher energy compared to the hydrogen atom in L^1. In contrast the electron-withdrawing phenyl group in L^3 induces a red shift in the $n \rightarrow \pi^*$ transition. This red shift can be attributed to the increased conjugation effect [42]. The absorption spectral data in Table 3 show that there is a significant change in the energy of $n \rightarrow \pi^*$ band on complexation. The band maximum in the spectra of the

Table 3
Elecronic absorption spectra (cm^{-1}) of oxidovanadium (IV) hydrazones.

Compound	$^2B_{2g} \rightarrow {}^2E_{2g}$	$^2B_{2g} \rightarrow {}^2B_{1g}$	$^2B_{2g} \rightarrow {}^2A_{1g}$	$n \rightarrow \pi^*$
L^1	12,987	17,241	23,529	31,746
(1)				27,027
L^2	13,072	18,181	25,000	33,222
(2)				28,571
L^3	12,903	16,949	22,522	29,239
(3)				25,641
L^4	13,037	17,271	24,570	30,769
(4)				27,777
L^5	13,055	17,391	23,809	31,847
(5)				27,397
L^6	13,245	17,857	24,691	33,112
(6)				28,985
L^7	13,333	18,348	25,316	32,051
(7)				28,169

Complex details are as listed in Table 1.

chelates is shifted to lower frequencies relative to those in the free ligands. This bathochromic shift may result from the extended conjugation in the ligand forced by the chelated metal ion.

The data in Table 3 reveal that the increasing energy order of the $n \rightarrow \pi^*$ bands of the reported oxidovanadium (IV) complexes: *(2) > (6) > (7) > (4) > (5) > (1) > (3)* reflects the decreasing order of Lewis acidity of the central VO^{2+} ion. This finding suggests that the strengths of the metal-ligand equatorial bonds increase in the above order. This trend may be attributed to the expected lower basicity of the imine nitrogen atoms when phenyl group is bonded to the carbon atom of the Schiff base linkage, as compared with methyl group with its inductive (electron releasing) effect.

3.4. Magnetic studies

Oxidovanadium (IV) ion belongs to the $3d^1$ and $S = 1/2$ system [43]. The observed magnetic moments of the reported oxidovanadium (IV) complexes *(2)*, *(3)*, *(6)* and *(7)* at room temperature lie in the 1.87–2.15 BM range, corresponding to one unpaired electron and consistence with the mononuclear monomeric structure of these complexes. This result is in accord with the fact that the spin-orbit coupling for oxidovanadium (IV) complexes is positive and the magnetically diluted oxidovanadium (IV) ion should exhibit magnetic moments very close to the spin-only value, as expected for a simple $S = 1/2$ paramagnetic with d_{xy} based ground state [44]. These normal magnetic moments excluded any significant interaction between neighboring oxidovanadium (IV) ions in the polycrystalline state [44]. This fact is also supported by the ESR spectral results (Table 4), which give *G*-values in the range 4.039–4.328, $[G = (g_{\|} - 2)/(g_{\perp} - 2)] > 4$ [45]. According to Hathaway et al. if the $G > 4$, the exchange interaction is negligible, while $G < 4$ indicates considerable exchange interaction in the solid complexes [45].

For the mononuclear complex *(6)* the magnetic moment value (2.15 BM) is markedly higher than the spin-only value for the magnetically dilute oxidovanadium (IV) complexes. This positive deviation from the spin-only value (1.73 BM) can be attributed to incomplete quenching of the orbital contribution to the magnetic moment in addition to the contribution from spin-orbit coupling [46].

The observed magnetic moment per metal ion in the dimeric molecule of complexes *(1)* and *(4)* (Table 4) is considerably less than the spin-only value for $S = 1/2$ usually observed in the absence of any exchange interaction. This lowering at room temperature reveals the presence of antiferromagnetic spin-exchange interaction between the two oxidovanadium (IV) centers through the bridging oxygen atom of the tridentate hydrazone ligand (Scheme 2**)**. In the oxo-bridged complexes the two metal atoms are drawn closer and a π–pathway for superexchange is expected. This should cause a quenching in the magnetic moment. Considering the splitting pattern of oxidovanadium (IV) the unpaired electron of the vanadyl (IV) ion will be located in the ground state orbital d_{xy} and the energy order of the *d* orbital is d_{xy} (↑) $< d_{xz}$ $d_{yz} < d_x{}^2{-}_y{}^2 < d_Z{}^2$. The oxygen atoms of the tridentate mono basic hydrazones (L^1 and L^4) act as bridges between the two oxidovanadium (IV) ions. Since it is the $d_x{}^2{-}_y{}^2$ orbital which faces the bridging oxygen atoms and since this orbital does not carry the unpaired spin, the spin–spin interaction cannot occur via the superexchange mechanism. Indeed, the dimeric formulation brings the two d_{xy} orbitals of the oxidovanadium (IV) ions so close to each other that the direct spin–spin interaction may proceed via the σ overlap of these two orbitals. The indirect π–pathway of superexchange through the $d_x{}^2$-$_y{}^2$ (V) P_Z (O) $d_x{}^2{-}_y{}^2$ (V) overlap is expected to be weak since the $d_{xy}-$, $d_x{}^2{-}_y{}^2$ mixing will only occur in the high energy state [44].

Table 4
Magntic moments and esr pectral data of oxidovanadium (IV) hydrazones.

Complex	$g_{\|}$	$g_{\perp}$	g_{av}	*G*	μ_{eff} (BM)
(1)	2.212	2.055	2.107	3.854	2.24
(2)	2.235	2.055	2.115	4.273	1.93
(3)	2.255	2.061	2.126	4.180	1.88
(4)	2.215	2.071	2.119	3.028	2.21
(5)	2.311	2.077	2.155	4.039	3.40
(6)	2.277	2.064	2.135	4.328	2.15
(7)	2.219	2.053	2.108	4.132	1.87

Complex details are as listed in Table 1.

Although, the binuclear complexes *(5)* is magnetically concentrated and it exhibits magnetic moment per oxidovanadium (IV) ion in the dimeric molecule close to the spin-only value of the magnetically dilute oxidovanadium (IV) complexes. This result indicates the absence of any spin–spin interaction between the two oxidovanadium (IV) centers in this binuclear chelate in the solid state. It is well known that for the magnetically concentrated binuclear complex the antiferromagnetic interaction path ways (direct metal–metal interaction or superexchange interaction) are highly sensitive to the metal–metal distance within the same molecule. A metal–metal distance less than a 4Å in the dimeric metal complex is usually indicative of the presence of magnetic exchange interaction [44]. In order to obtain further structural information and due to the lack of X-ray and variable temperature magnetic susceptibility measurements facilities in our laboratory, the ESR spectra of the reported oxidovanadium (IV) hydrazones were measured and the V–V distance in the dimeric complexes *(1)*, *(4)* and *(5)* was determined. As well as, the magnetic exchange interaction parameter, *J*, for the investigated dimeric complexes *(1)*, *(4)* and *(5)* was computed from the ESR measurements.

The X-band ESR spectra of the synthesized oxidovanadium (IV) complexes in the polycrystalline state have been recorded at room temperature. A representative spectrum is shown in Fig. 1. However, the spectra of complexes *(1)* – *(7)* are anisotropic, having parallel and perpendicular features (Fig. 1). The $g_{\|}$ and $g_{\perp}$ values are computed from the spectra using DPPH free radical as g-marker and the results are given in Table 4. The ESR spectra are interpretable in terms of an effective spin of $S = 1/2$, and $I = 7/2$. The trend $g_{\|} > g_{\perp} > g_e$ (2.0023) observed for the investigated complexes shows that the unpaired electron of the d^1 (VO^{2+}) is located in the d_{xy} orbital and the spectral features are characteristic of axially elongated square pyramidal geometry [44]. These spectral features can be assigned unambiguously to oxidovanadium (IV) ions in the form of single and or pair ions by comparison with spectra of such species in other matrices [47,48].

As indicated by the magnetic moment measurements there seems to be no exchange interaction between the oxidovanadium (IV) ions in the solid state of complexes *(2)*, *(3)*, *(5)*, *(6)*, and *(7)*. This fact is further confirmed by the ESR spectral data which give *G* values in the range 4.039–4.328 > 4.0 [49]. This fact reveals that these complexes are monomeric in nature and the metal–metal interactions are absent. However, the monomeric or dimeric nature of the reported oxidovanadium (IV) hydrazone complex molecules can be distinguish by employing the ESR spectroscopy at room temperature. It is well-known that the ESR spectrum of a pair is radically different from that of a single ion, since at a certain distance between the two oxidovanadium (IV) ions forming the pair, the coupling between the two unpaired electrons becomes significant and the system splits into a triplet state ($S = 1$) and a singlet state ($S = 0$). Only the triplet state is paramagnetic giving in ESR, two signals corresponding to allowed transitions ($\Delta Ms = 1$) and one signal corresponding to a forbidden transition ($\Delta Ms = 2$). Depending on the microwaves frequency, the most visible EPR characterization of VO^{2+} pairs existence is the presence of weak signal at half normal field intensity, produced by forbidden transition [49]. The inter-ion distance in the pair, *R*, can be determined [50], from the relative intensity *I* between the signal observed at $\Delta Ms = 2$ (forbidden transition) and that obtained at $\Delta Ms = 1$ (allowed transition):

$$I = A(9.1)^2 / \left(R^6 \upsilon^2\right)$$

where *A* is a constant, *R* is the inert ion distance in Å and υ is the measuring microwave frequency in GHz.

When a pair signal is anisotropic with axial symmetry, one can deduce directly the values $d_{\|}$ and $d_{\perp}$. These parameters are defined by:

$$d_{\|} = 2D/g_{\|}\ \beta \text{ and } d_{\perp} = 2D/g_{\perp}\ \beta$$

where *D* is the zero field splitting constant and β is the Bohr magnetone. The average distance between the two oxidovanadium (IV) ions in the dimeric complexes *(1)*, *(4)* and *(5)* can be calculated from the zero - field splitting (*D* term) values by using the equation [44]:

$$R^3 = 3g_{\|}^2\ \beta^2/2D.$$

Also the ESR spectral results were employed to calculate the exchange coupling constant *J* which measures the extent of the antiferromagnetism behavior of the dimeric transition metal complexes. The relative intensity (*I*) of absorption of the esr lines is related to *J* as [44]

$$I = 1/T\ (e^{[-J/(kT)]}/1 + 3\ e^{[-J/(kT)]})$$

The data in Table 4 demonstrate that, the magnetic exchange interaction for the three dimeric complexes *(1)*, *(4)* and *(5)* seems to depend on the metal–metal distance, i.e. the shorter the metal distance in the dimeric metal complex the stronger is the antiferromagnetic interaction. A comparison of the *J* values and the V–V distance (*R*) in the dimeric complexes *(1)* ($J = -148\ cm^{-1}$, $D = 0.0479\ cm^{-1}$, $R = 3.97$Å), *(4)* ($J = -138\ cm^{-1}$, $D = 0.0521\ cm^{-1}$, $R = 3.94$ Å) and *(5)* ($J = -97\ cm^{-1}$, $D = 0.0339\ cm^{-1}$, $R = 4.68$ Å) indicates that the antiferromagnetic exchange interaction increases with the decrease in the V–V distance. This shows that the contribution to singlet–triplet separation from a direct metal–metal bond is significant and the exchange interaction occurs predominately through the direct metal–metal interaction mechanism.

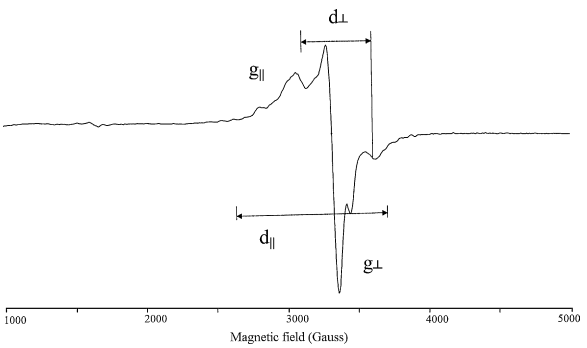

Fig. 1. ESR spectrum of oxidovanadium (IV) complex (1).

All our efforts to grow crystals of these oxidovanadium (IV) complexes suitable for X-ray structure determination so far have been unsuccessful. However, based on the composition of these complexes, their IR and electronic spectra, conductivity measurements, magnetic studies (vide supra), these complexes are proposed to have a square-pyramidal environment, as shown in Scheme 2. The plausible structure is further illustrated by the following thermal studies.

3.5. Thermal studies

3.5.1. Thermogravimetric analysis (TGA–DTG)

Thermogravimetric analysis was employed to clarify the nature of water content in the complex molecule. The decomposition stages temperature ranges, maximum decomposition peaks DTG_{max}, percentage losses in mass, and the assignment of decomposition moieties are given in Appendix A: supplementary material (S1). Typical TG and DTG plots for some complexes are given in Appendix A: supplementary material (S2). The thremogravimetric curves of complexes *(1)* – *(7)* are similar and show two stages of decomposition within the temperature range of ambient temperature to 670 °C. The first stage at 55–160 °C shows the first dehydration process associated with the loss of one to three molecules of water followed by the second stage at 160–240 °C temperature range, corresponding to loss of remaining water molecules supporting the presence of water bound in different ways: lattice and coordinated to the VO^{2+} ions. The number of these two kinds of water molecules per mole of metal ion was calculated form the weight loss observed for the complexes at these two temperature ranges and the results are given in Appendix A: supplementary materials. The second stage corresponds to the complete removal of the organic portion in addition to the counter ion SO_4^{2-}, in successive decomposition steps within the temperature range 240–670 °C leaving the metallic oxide (V_2O_5) as a residual. The observed overall weight loss amounts (Appendix A: supplementary materials) are in a good agreement with the calculated values based on the suggested formulae of these complexes and consistent with the thermal material decomposition and elimination of the complex molecule contents.

3.5.2. Kinetic aspects

The kinetic activation parameters of the thermal decomposition of the investigated oxidovanadium (IV) complexes, are evaluated graphically by using the Coats-Redfern method [51], and the results obtained are given in Appendix A: supplementary material (S1). The thermodynamic parameters of the TGA studies permit coordinated and uncoordinated water molecules, to distinguish. The TG curves of the reported complexes demonstrated that, two thermal processes can be observed: (a) dehydration and (b) pyrolytic decomposition. The first and the second stages that take place in thermal decomposition of the complexes *(1)* – *(7)* are assigned to the dehydration processes of the outer sphere and the coordinated water molecules. On comparing the activation energy (E^*) and the dehydration enthalpy (ΔH^*) values (Appendix A: supplementary material S2) of the first and the second dehydration stage, the second stage shows remarkable higher values. For all dehydrated complexes, the thermodynamic parameters values of the pyrolytic decomposition stage were found to be higher than that of the dehydration stage which indicates that the rate of the pyrolytic stage is lower than that of the dehydration stage.

3.6. Electrochemical studies

The electrochemistry of the synthesized oxidovanadium (IV) complexes was investigated as the redox potential is an important parameter in the electron transfer reactions we are studying. The redox potential should be such as to permit the reoxidation of the reduced oxovanadium centers by molecular oxygen to maintain the catalytic cycle.

The redox properties of the investigated oxidovanadium (IV) hydrazones were investigated in DMF solution (in a nitrogen atmosphere) by cyclic voltammetry and the redox processes are metal centered only (Table 5). Cyclic voltammograms of the entire complexes (1×10^{-3} M) exhibit a reversible oxidation and reversible reduction peaks at the scan rate 100 mV s^{-1}. All the complexes showed well-defined waves in the range ($E_{1/2}$) 0.0.372 to 0.507 V of the couple (VO^{IV}/VO^{III}) *versus* Ag/AgCl. The redox processes are reversible with peak-to-peak separation (ΔE_p) values ranging from 59 to 85 mV. The peak potentials separation and the ratio of cathodic to anodic peak current are close to unity consistent with one-electron process. This indicates that the electron transfer is reversible and the mass transfer is limited. The electrode processes can be described by the following equation;

$$\left[LVO^{IV}\right] + e \rightleftharpoons \left[LVO^{III}\right]$$

The data in Table 5 reveal that the nature of substitution on the Schiff- base linkage has a significant effect on $E_{1/2}$ of

Table 5
Electrochemical data (scan rate of 100 V/s) and catechol oxidase biomimetic catalytic activity of the oxidovanadium (II) hydrazones.

Complex	E_{pc}	E_{pa}	ΔE_p/mV	i_c/i_a	$E_{1/2}$/V	*TR*	$K_{obs} \times 10^3$
(1)	0.344	0.402	59	1.18	0.372	23.99	56.79
(2)	0.464	0.549	85	1.17	0.507	12.98	30.64
(3)	0.408	0.478	70	1.13	0.443	6.35	14.86
(4)	0.416	0.499	83	1.02	0.457	17.36	41.0
(5)	0.329	0.412	83	1.25	0.370	19.76	47.0
(6)	0.482	0.558	75	1.13	0.520	9.88	23.4
(7)	0.349	0.429	80	1.1	0.389	15.95	38.0

Complex details are as listed in Table 1.

the reported complexes. The electron-withdrawing groups stabilize the lower oxidation state V^{3+} in the complex *(3)* while the electron-donating group favor oxidation to $V^{(IV)}$ in the complex *(2)*. This is possibly because the electron-withdrawing phenyl ring makes the complex more positively charged and hence causes it to be more easily reduced. Similarly the electron-donating groups as inductive or mesomeric (CH_3) make the complexes *(2)* and *(6)* less positively charged and hence less easily reduced. On the other hand the data in Table 5 demonstrated that, the difference in the redox potential values of complexes *(1)* and *(4)* is strongly related to the basicity of the donor atoms of the coordination environment around the central oxidovanadium (IV) ion. The coordination chromofore of complex *(1)* is NNOO while for complex *(4)* is NSOO, and the later comprises the more basic sulfur donor. Thus, complexes formed with donor atoms possessing a high electron density (basicity) will show higher $E_{1/2}$ values than that formed with weaker bases. Cyclic voltammetry results of the reported oxidovanadium (IV) complexes reveal a reduction potential values in the range expected for the five-coordinated mono oxidovanadium species on the basis of other members in this series [40c,e,f,48,52,53]. The fact that the reduction is completely reversible indicates that the five-coordinate geometry is stable in both oxidation states, at least on the cyclic voltammetry time scale [52,53].

3.7. Catechol oxidase biomimetic catalytic activity

The oxidase biomimetic catalytic reactivity of the reported oxidovanadium (IV) complexes *(1)* – *(7)* towards the aerobic oxidation of 4-*tert*-butylcatechole under catalytic conditions was studied using electronic spectroscopy by following the appearance of the absorption maximum of the quinone at 400 nm over time. Some of the obtained results are illustrated in Figs. 2 and 3, showing the change in absorbance at 400 nm versus time for the first 30 min. Also, the catalytic activities were evaluated from the relation: [turn over rate (TR) = mole of *o*-quinone produced per mole of catalyst per minute], by making use

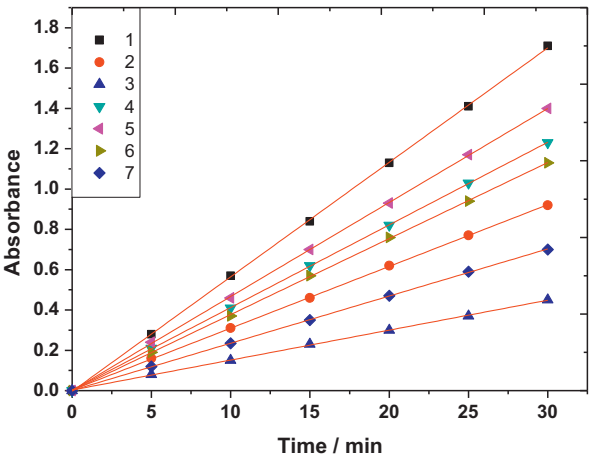

Fig. 2. Kinetic curves of the catalyzed oxidation of 4-*tert*-butylcatechol in the presence of oxidovanadium (IV) complexes *(1)*–*(7)*, monitored at 400 nm.

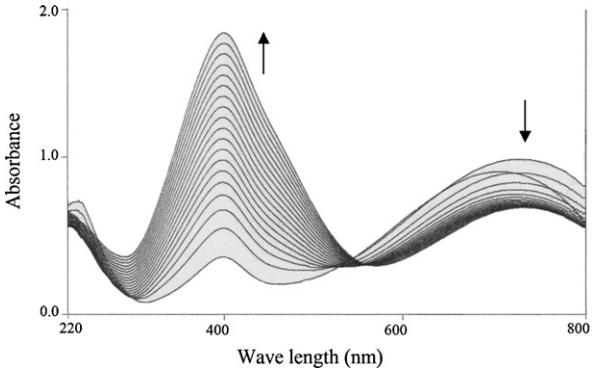

Fig. 3. Spectral changes observed in the oxidation reaction of 4-*tert*-butylcatechol catalyzed by complex *(1)*.

of molar absorbance value of $\varepsilon = 1200\ M^{-1}\ cm^{-1}$ reported by Munoz et al. [54]. The results obtained are presented in Table 5 and it is clear that there are profound differences in the ability of the complexes to catalyze the oxidation reaction. There are a number of factors which need to be considered in explaining the differences in the catalytic properties of complexes *(1)*–*(7)*. These include (a) the electrochemical properties of the complexes, (b) the geometry imposed by the ligands on the metal ion, (c) the Lewis acidity of the oxidovanadium (IV) center created by the donating properties of the primary hydrazone ligands, (d) the basicity of the donor atoms and (e) the steric features of the ligands. All of these factors will be considered sequentially.

3.7.1. Electrochemical considerations

Electrochemistry was used to establish whether there is a correlation between the redox potential and catecholase biomimetic catalytic capabilities of the synthesized oxidovanadium (IV) complexes. It should be noted that the enzyme tyrosinase (catalyzes the aerobic oxidation of catechole to the light absorbing *o*-quinone) isolated from mushroom (*Agaricus bisporus*) has a reported value for E° of 0.36 V vs. the standard calomel reference [55]. It is obvious however, that the enzyme has been able to balance successfully the requirements of the different oxidation states of the metal $M^{n+} \rightleftharpoons M^{(n-1)+}$ in performing its catalytic tasks. The balance between ease of reduction of oxidovanadium (IV) and subsequent reoxidation oxidovanadium (III) by molecular oxygen must be maintained for efficient catalysis to occur. This would imply that a window of $E_{1/2}$ values exists wherein effective catalysis can take place. If the reduction potential is too negative, reduction to oxididovanadium (III) be unattainable; on the other hand, if the reduction potential is too positive, the catalytic cycle would be short-circuited because once reduced to $V^{(III)}$, the complexes would be unable to be easily reoxidized to $V^{(IV)}$ by O_2.

A comparison of the $E_{1/2}$ values for the seven complexes studied with the observed catalytic properties yields a number of interesting results. First, the four complexes *(1)*, *(4)*, *(5)* and *(7)* with appreciable activity in the aerobic oxidation of catechole have $E_{1/2}$ values approaching the E° value of the natural tyrosinase enzyme. On the other hand

complex *(6)* exhibits $E_{1/2}$ value that deviate from that potential and consequently this leads to significant loss of activity. This finding suggests that, within a certain range of $E_{1/2}$ values appreciable catalysis is possible, while outside that range the drop off in rate is quite significant.

While our data do suggest an interdependency between the catalytic properties of the complexes and their redox potentials, it is clear that electronic effects do not totally control the reactivity and that other factors are also at work in the catalytic cycle. This is best illustrated by examining the reactivity of complexes *(3)* and *(4)* which have virtually identical reduction potentials but enormously different rates of catalytic oxidation reaction. This finding is also observed for other examples of copper(II) complexes which have essentially identical reduction potentials but drastically different catalytic properties [56].

3.7.2. Geometrical considerations

As shown in Table 5, the square-pyramidal complexes *(1)–(7)* catalyze the aerobic oxidation reaction. Therefore, the five-coordinate, square-pyramidal complexes *(1)–(7)* are capable of serving as catalysts for oxidation reactions so other factors must be responsible for the differences in rate.

3.7.3. Basicity of the donor atoms

The third consideration in assessing the reactivity of these complexes is the basicity of the donor atoms. This feature will affect the Lewis acidity of the central oxidovanadium (IV) and consequently the redox potentials of the complexes by shifting the $E_{1/2}$ values of complexes. It has been previously reported that the nature of the donor atoms, the counter ion, or any bridging group bound to the metal centers has an effect on the rate of catalysis [57,58]. In addition, it has been shown that electron transfer from catechole to LM^{n+} can begin only after catechol and the LM^{n+} species form an LM^{n+}-catecholate intermediate [59]. Accordingly, the initiation step almost certainly involves production of V^{3+} by the interaction of oxidovanadium (IV) complex with catechol. In this situation, the V^{3+}/V^{4+} couple is involved as a redox center. According to the mechanistic hypothesis, the Lewis acidity of a oxidovanadium (IV) center in the oxidovanadium (IV)-catecholate intermediate greatly affects the redox potential of the V^{3+}/V^{4+} couple and consequently degree of the catalytic reactivity. Thus, an increase in the Lewis acidity of the oxidovanadium (II) center in the $[(VOL^n)_2-$catecholae] complex facilitates electron transfer from the catecholate ring to the oxidovanadium (IV) center. For *(1)* and *(2)* complexes, the electronic absorption spectra exhibit a charge transfer band assignable to $n \rightarrow \pi^*$ of the azomethine linkage of the hydrazone ligands. The position and intensity of this band show dependence on the type of substituents within the carbonyl moiety of the imine ligands. The increasing order of this energy (*(2) > (1)*) reflects the decreasing order of the Lewis acidity of the oxidovanadium (IV) center [27,60]. The presence of the electron-donating group (CH_3) in L^2 increases the Lewis basicity of the donor nitrogen atoms and shifts the $n \rightarrow \pi^*$ band of the C=N to higher energy (Table 3). Thus, the Lewis acidity, as shown by the C.T. $n \rightarrow \pi^*$ band energy, increases in the order: *(1) > (2)* and the catalytic reactivity of these complexes follow the same order. Consequently, in the $[(VOL^n)_2-$catecholae] intermediate, electron transfer from the catecholate ring to the complex *(1)* center is assumed to be more favored as compared with complex *(2)*. In contrasting complexes *(5)* with *(6)* it can be seen that this is the case. These data are consistent with the premise that the basicity of the donor atoms is one of the primary factors in modulating the resultant electrochemical properties of the complexes.

3.7.4. Steric features of the ligands

The data in Table 5 shows that oxidovanadium (IV) center in the VOL^3 complex has a Lewis acidity value greater than that of the *(4)*. Although complexes *(3)* and *(4)* have virtually identical redox potential (Table 5), but the latter *(4)* is significantly more reactive. Since the electrochemical and the spectral results seem to minimize the importance of electronic factors, we will consider the role of the complexes structural features on their catalytic reactivity properties. Our results point to the bulky ligand environment provided by the L^3 (which has extra phenyl group on the Schiff base linkage as compared to L^4) will being responsible for the diminution of its rate of catalysis compared to L^4. For these systems, it seems that as the ligand becomes more crowded, the substrate is less able to coordinate to the metal ion and, as a result, the catalytic process is slowed down.

3.7.5. Suggested mechanism for the catalytic oxidation of catechol

The possible mechanistic implications (Scheme 3) whereby the oxidovanadium (IV) complexes catalyze the oxidative transformation of catechol to the light absorbing *o*–quinone presumably implies the following interactions: (i) Formation of dioidxovanadium (IV)-catecholate intermediate; such an intermediate is well known in analogous oxidase model systems [27,60b,61]. (ii) The formation of this intermediate was proposed previously as the rate-determining step in the oxidation process, which undergoes further fast reactions to the final oxidation product and two $M^{(n-1)+}$ centers [61]. This was demonstrated by the spectral changes with time (Supplementary data). The absorption band at 756 nm, attributed to $[(VO^{(IV)}L)_2-$catecholate] intermediate adduct, decreases while the band at 400 nm, due to the formation of *o*-quinone, increases more rapidly with an isosbestic point at about 560 nm. The final spectrum of the system contains a band at 400 nm characteristic of *o*-quinone and the 765 nm band of the oxidovanadium (IV)–catecholate intermediate adduct complex. This intermediate could be recognized under intermolecular electron-transfer to the oxidized *o*-quinone product and two oxidovanadium (III) centers. (iii) Interaction of the generated oxidovanadium (III) species with O_2 to give *cis*- μ-η^1: η^1 or a -μ-η^2: η^2 peroxide adduct $[(LVO^{IV})_2O_2]$. This process presumably involves the transfer of an electron from the oxidovanadium (III) ion. Previously reported studies involving catecholase functional models complexes catalyzing the oxidation of catechols suggested the formation of dimeric species, in the rate-determining step [60b,62]. Accordingly, the initiation step

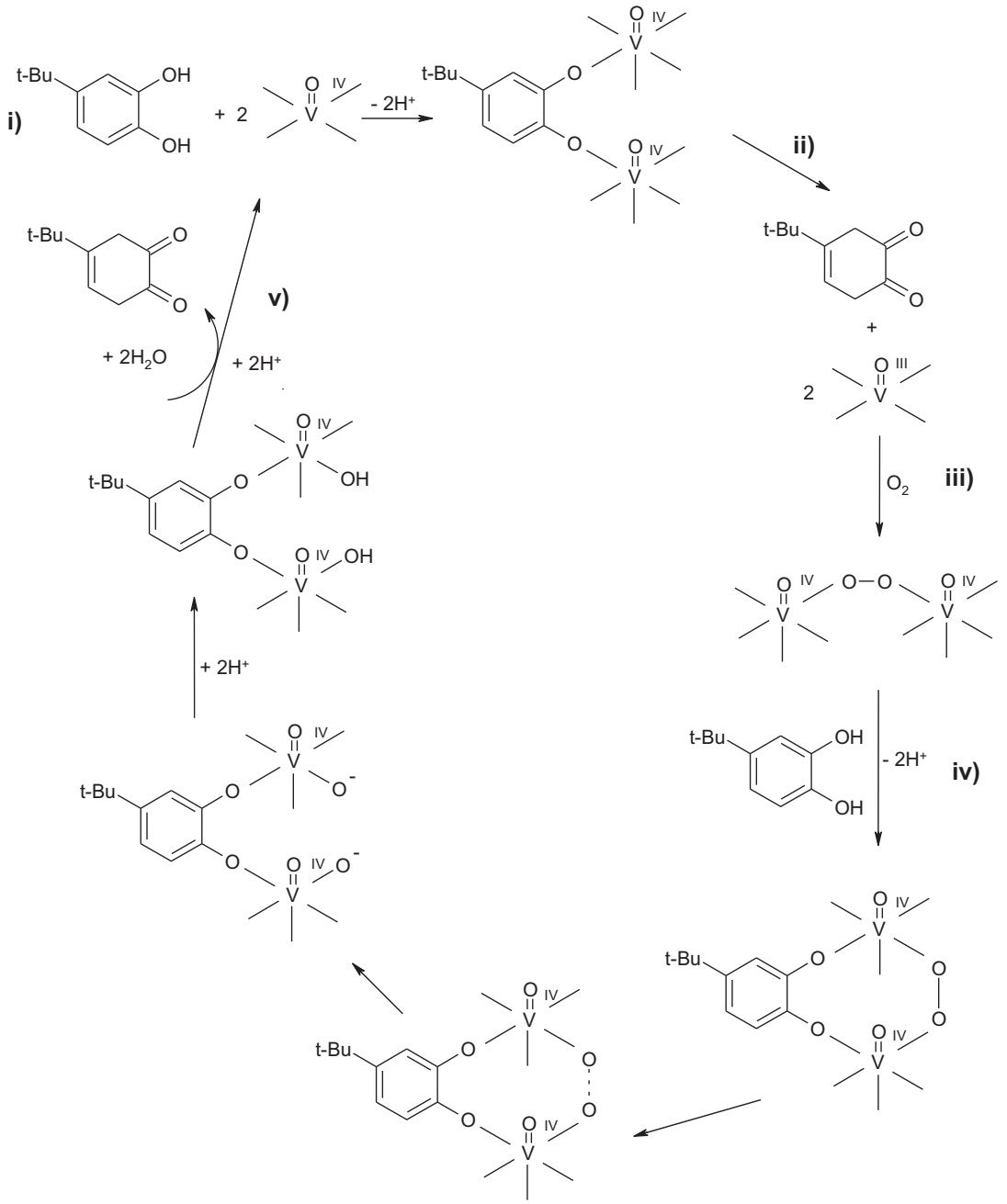

Scheme 3. Mechanism of the aerial oxidation of 4-tert-butylcatechol by oxidovandium (IV) picolyl hydrazones.

almost certainly involves production of oxidovanadium (III) by the interaction of the oxidovanadium (IV) with catechol. In this situation, the VO^{IV}/VO^{III} couple is involved as a redox center. (iv) Interaction between the more basic and highly reactive catecholate radical and $[(LVO^{IV})_2O_2]$ leads to the formation of [catecholate $(LVO^{IV})_2O_2$] adduct. As a consequence of these interactions, the resulting adduct [catecholate $(LVO^{IV})_2O_2$] undergoes rearrangement to give an oxide anion, which remains coordinated to the oxidovanadium (IV) center. The protonation of O^{2-} prior to its release from the complex is required, because the oxide anion is highly basic and thus too unstable to be released in its unprotonated form. Thus, we suggest that the oxide fragment rearranges to the hydroxide radical (HO^-) as a result of the electrophilic attack by a proton on the highly basic oxide anion bound to oxidovanadium (IV) provides the HO^- radical. (v) Finally, this intermediate could be recognized under further electrophilic attack by a proton on the highly basic hydroxide anion bound to oxidovanadium (IV) to the totally oxidized form *o*-quinone and two water molecules as a by-product and regeneration of the catalyst in its original active form (Scheme 3).

4. Conclusion

The present study describes the syntheses and characterization of a series of oxidovanadium (IV) complexes with the tridentate picolyl hydrazones ligands. The structural characterization of the synthesized compounds was achieved by several physicochemical methods namely, elemental analysis, thermal studies, magnetic, electrochemical and spectroscopic techniques. The reported oxidovanadium (IV) complexes contain a five-coordinated vanadium (IV) ion in an oxygen and nitrogen rich environment in the square–pyramidal geometry. A monomeric nature was reported for complexes *(2)*, *(3)*, *(6)* and *(7)* while dimeric structures were suggested for complexes *(1)*, *(4)* and *(5)*. The catechol oxidase biomimetic catalytic activity of the synthesized complexes has been investigated. The results obtained show that all the complexes catalyze the aerobic oxidation of catechol to the corresponding light absorbing *o*-quinone. The rate of catalysis for the investigated oxidovanadium (IV) complexes is linked to the redox potential of the couple V^{3+}/V^{4+} during the catalytic cycle, the Lewis basicity of the donor atoms and the steric features of the parent ligand. A substantial retardation of reactivity is evident if either steric or electronic factors are not optimal.

Appendix A. Supplementary data

Supplementary data (Tables S1 and S2) associated with this article can be found, in the online version, at doi:10.1016/j.crci.2011.11.009.

References

[1] (a) O. Bortolini, V. Conte, J. Inorg. Biochem. 99 (8) (2005) 1549;
(b) A. Butler, J.N. Carter-Franklin, Nat. Prod. Rep. 21 (1) (2004) 180;
(c) J.M. Winter, B.S. Moore, J. Biol. Chem. 10 (284) (2009) 18577;
(d) M. Rangel, M.J. Amorim, A. Nunes, A. Leite, E. Pereira, B. de Castro, C. Sousa, Y.M. Hiromura, H. Sakurai, Chem. Biodivers. 5 (8) (2008) 1615.

[2] (a) T. Ohshiro, J. Littlechild, E. Garcia-Rodriguez, M.N. Isupov, Y. Iida, T. Kobayashi, Y. Izumi, Protein Sci. 13 (6) (2004) 1566;
(b) J. Littlechild, E. Garcia Rodriguez, M. Isupov, J. Inorg. Biochem. 103 (4) (2009) 617;
(c) J.N. Carter-Franklin, J.D. Parrish, R.A. Tschirret-Guth, R.D. Little, A. Butler, J. Am. Chem. Soc. 2 (125) (2003) 3688;
(d) S. Barroso, P. Adão, F. Madeira, M.T. Duarte, J.C. Pessoa, A.M. Martins, Inorg. Chem. 16 (49) (2010) 7452;
(e) H. Yoshikawa, H. Sakurai, J. Inorg. Biochem. 103 (4) (2009) 496.

[3] (a) M.R. Maurya, A. Kumar, M. Ebel, D. Rehder, Inorg. Chem. 24 (45) (2006) 5924;
(b) M.R. Maurya, M. Bisht, A. Kumar, M.L. Kuznetsov, F. Avecilla, J.C. Pessoa, Dalton Trans. 14 (40) (2011) 6968;
(c) M.R. Maurya, A. Arya, U. Kumar, A. Kumar, F. Avecilla, J.C. Pessoa, Dalton Trans. 21 (43) (2009) 9555;
(d) M.R. Maurya, A.A. Khan, A. Azam, S. Ranjan, N. Mondal, A. Kumar, F. Avecilla, J.C. Pessoa, Dalton Trans. 7 (39) (2010) 1345;
(e) P. Adão, J. Costa Pessoa, R.T. Henriques, M.L. Kuznetsov, F. Avecilla, M.R. Maurya, U. Kumar, I. Correia, Inorg. Chem. 20 (48) (2009) 3542;
(f) H.S. Seleem, M.A. Mousa, Chem. Cent. J. 16 (5) (2011) 47.

[4] K.H. Thompson, C. Orvig, Coord. Chem. Rev. 219 (2001) 1033.

[5] H. Sakurai, Y. Kojima, Y. Yoshikawa, K. Kawabe, H. Yasui, Coord. Chem. Rev. 226 (2002) 187.

[6] R. Wever, W. Hemrika, A. Messerschmidt, R. Huber, T. Poulos, K. Wieghardt (Eds.), Handbook of Metalloproteins, Vol. 2, Wiley, Chichester, 2001, p. 1417.

[7] A. Butler, C. Opin, Chem. Biol. 2 (1998) 279.

[8] A. Butler, M.J. Clague, G.E. Meister, Chem. Rev. 94 (1994) 625.

[9] A. Butler, J.V. Walker, Chem. Rev. 93 (1993) 1937.

[10] H. Vilter, in: H. Sigel, A. Sigel (Eds.), Metal Ions in Biological systems Vol. 31, Marcel Dekker, New York, 1995, p. 325.

[11] V. Conte, F. Di Furia, G. Licini, Appl. Catal. A 157 (1997) 335.

[12] S. Mohebbi, D.M. Boghaei, A.H. Sarvestani, Appl. Catal. A 278 (2005) 263.

[13] W. Zhang, A. Basak, Y. Kosugi, Y. Hoshino, H. Yamamoto, Angew. Chem. Int. Ed. Engl. 44 (2005) 4389.

[14] J.H. Hwang, M. Abu-Omar, Tetrahedron Lett. 40 (1999) 8313.

[15] E. Battistel, R. Tassinari, M. Fomaroli, L. Bonoldi, J. Mol. Catal. A 202 (2003) 107.

[16] G.B. Shul'pin, G. Suss-Fink, J. Chem. Soc. Perkin Trans. 2 (1995) 1459.

[17] A. Barbarini, R. Maggi, M. Muratori, G. Sartori, R. Sartorio, Tetrahedron Asym. 15 (2004) 2467.

[18] T.S. Smith, V.L. Pecoraro, Inorg. Chem. 41 (2002) 6754.

[19] R. Ando, T. Yagyu, M. Maeda, Inorg. Chim. Acta 357 (7) (2004) 223.

[20] S.R. Reddy, S. Das, T. Punniyamurthy, Tetrahedron Lett. 45 (2004) 3561.

[21] E. Hoppe, C. Limberg, B. Ziemer, Inorg. Chem. 45 (2006) 8308.

[22] P.J. Figiel, J.M. Sobczak, J.J. Ziolkowski, Chem. Commun. 2 (2004) 244.

[23] R.R. Eady, Coord. Chem. Rev. 237 (2003) 23.

[24] (a) M. Weyand, H.J. Hecht, M. Kiess, M.F. Liaud, H. Vitler, D. Schomburg, J. Mol. Biol. 293 (1999) 595;
(b) W. Plass, Angew. Chem. Int. Edn. Eng. 38 (1999) 909.

[25] (a) J.N. Carter-Franklin, J.D. Parrish, R.A. Tchirret-Guth, R.D. Little, A. Butler, J. Am. Chem. Soc. 125 (2003) 3688;
(b) D. Rehder, G. Antoni, G.M. Licini, C. Schulzke, B. Meier, Coord. Chem. Rev. 237 (2003) 53.

[26] (a) A. Pohlmann, S. Nica, T.K.K. Luong, W. Plass, Inorg. Chem. Commun. 8 (2005) 289;
(b) W. Plass, Coord. Chem. Rev. (2003) 237;
(c) S. Nica, A. Pohlmann, W. Plass, Eur. J. Inorg. Chem. 205 (2005) 2032;
(d) T. Ghosh, Transition. Met. Chem. 31 (2006) 560;
(e) W. Plass, A. Pohlmann, H.P. Yozgatli, J. Inorg. Biochem. 80 (2000) 181;
(f) N.R. Sangeetha, S. Pal, Bull. Chem. Soc. Jpn 73 (2000) 357;
(g) R. Dinda, P. Sengupta, S. Ghosh, T.C.W. Mak, Inorg. Chem. 41 (2002) 1684.

[27] A.M. Ramadan, R.M. Issa, Transition Met. Chem. 30 (2005) 471.

[28] T. Ghosh, C. Bandyopadhyay, S. Bhattacharya, G. Mukherjee, Transition Met. Chem. 29 (2004) 444.

[29] M.R. Maurya, S. Khurana, C. Schulzke, D. Rehder, Eur. J. Inorg. Chem. (2001) 779.

[30] V. Vcrgopoulos, W. Priebsch, M. Fritzsche, D. Rehder, Inorg. Chem. 32 (1993) 1844.

[31] R.H. Clark, E.S. Williams, Inorg. Chem. 4 (1965) 350.

[32] K. Nakamoto, Infrared and Raman spectra of inorganic and coordination compounds, Wiley, New York, 1986.

[33] R.C. Maurya, P. Patel, Spectrosc. Lett. 32 (2) (1999) 213.

[34] (a) E.B. Seena, N. Mathew, M. Kuriakose, M.R.P. Kurup, Polyhedron 27 (2008) 1455;
(b) B. Mondal, T. Ghosh, M. Sutradhar, G. Mukherjee, M.G.B. Drew, T. Ghosh, Polyhedron 27 (2008) 2193;
(c) N.A. Mangalam, S. Sivakumar, S.R. Sheeja, M.R.P. Kurup, E.R.T. Tiekink, Inorg. Chim. Acta 362 (2009) 4191.

[35] S.K. Dutta, S.B. Kumar, S. Bhattacharyya, E.R.T. Tiekink, M. Chaudhury, Inorg. Chem. 36 (1997) 4954.

[36] A.B.P. Lever, Inorganic Electronic Spectroscopy, Elsevier, Amsterdam, 1968.

[37] C.J. Ballhausen, H.B. Gray, Inorg. Chem. 1 (1962) 111.

[38] L.G. Vanquickenbourne, S.P. McGlynn, Theor. Chim. Acta 9 (1968) 390.

[39] C.J. Ballhausen, Introduction to Ligand Field Theory, McGraw-Hill, New York, 1962.

[40] (a) M. Tumer, H. Koksal, M.K. Sener, S. Serin, Transition Met. Chem. 24 (1999) 414;
(b) N.M. El-Metwally, M. Issam, A.A. Gabr, El-Asmy, Transition Met. Chem. 31 (2006) 71;
(c) S. Zhan, C.W. Yuan, Transition Met. Chem. 24 (1999) 277;
(d) M.R. Maurya, P. Sweta Sikarwar, Manikandan, App. Catal. A Gen. 315 (2006) 74;
(e) N. Raman, S.J. Raja, J. Joseph, J.D. Raja, Koord. Khim. 33 (1) (2007) 7;
(f) G. Asgedom, A. Sreedhara, J. Kivikoski, C.P. Rao, Polyhedron 16 (4) (1997) 643;
(g) K.S. Abu-Melha, N.M. El-Metwally, Spectrochim. Acta Part A 70 (2008) 277.

[41] (a) D.X. West, A.A. Nassar, F.A. El-Saied, M.I. Ayad, Transition Met. Chem. 23 (1998) 321 [23, (1998) 423];
(b) D.X. West, D.L. Huffman, J.S. Saleda, A.E. Liberta, Transition Met. Chem. 16 (1991) 565;
(c) D.X. West, I. Thientaravanich, A.E. Liberia, Transition Met. Chem. 20 (1995) 303.

[42] (a) J.J. Lopaez-Carriga, G.T. Babcock, J.F. Harrison, J. Am. Chem. Soc. 108 (1986) 7241;
(b) S. Gourbatsis, S.P. Perlepes, N. Hadjilidis, Transition Met. Chem. 15 (1990) 300.
[43] B.N. Figgis, J. Lewis, Prog. Inorg. Chem. 6 (1964) 37.
[44] R.L. Dutta, A. Syamal, Elements of Magnetochemistry, 2nd ed., Alffiliated East-West Press, Delhi, 2007.
[45] B.J. Hathaway, O.E. Billing, Coord. Chem. Rev 5 (1970) 143.
[46] (a) J. Selbin, Chem. Rev. 65 (1965) 253;
(b) A. Syamal, Coord. Chem. Rev. 16 (1975) 309.
[47] B.T. Taker, A. Patel, L. Singh, Transition Met. Chem. 19 (1994) 623.
[48] N.M. El-Metwally, I.M. Gabr, A.A. El-Asmy, A.A. Abou-Hussen, Transition Met. Chem. 31 (2006) 71.
[49] R.C. Aggarwal, N.K. Singh, R.P. Singh, Inorg. Chem. 20 (1981) 2794.
[50] S.S. Eaton, K.M. More, B.M. Sawant, G.R. Eaton, J. Am. Chem. Soc. 105 (1983) 6560.
[51] A.W. Coats, J.P. Redfern, Nature 201 (1964) 68.
[52] N. Deligonul, M. Tumer, S. Serin, Transition Met. Chem. 31 (2006) 920.
[53] J.A. Bonadies, C.J. Carrano, J. Am. Chem. Soc. 108 (1986) 4088.
[54] J.L. Munoz, F. Garcia-Molina, R. Varon, J.N. Rodriguez-Lopez, F. Garcıa-Canovas, J. Tudela, Anal. Biochem. 351 (2006) 128.
[55] N. Makino, P. McMahill, H.S. Mason, J. Biol. Chem. 249 (1974) 6062.
[56] (a) N. Oishi, Y. Nishida, K. Ida, S. Kida, Bull. Chem. Soc. Jpn. 53 (1980) 2847;
(b) M.R. Malachowski, H.B. Huynh, L.J. Tomlinson, R.S. Kelly, J.W. Furbeejun, J. Chem. Soc. Dalton Trans. 31 (1995).
[57] A. Voldeba, W.G.J. Hol, J. Mol. Biol. 209 (1989) 249.
[58] J.E. Solomon, M.J. Baldwin, M.D. Lowery, Chem. Rev. 92 (1992) 521.
[59] J.M.M. Rogic, M.D. Swerdloff, T.R. Demmin, K.D. Karlin, J. Zubieta (Eds.), Copper Coordination Chemistry: Biochemical and Inorganic Perspectives, Adenine, Guilderland, NY, 1983, p. 167.
[60] (a) D. Cox, L. Que, J. Am. Chem. Soc. 110 (1988) 8085;
(b) A.M. Ramadan, I.M. El-Mehasseb, Transition Met. Chem. 23 (1998) 183.
[61] A.L. Abuhijleh, Polyhedron 15 (2) (1996) 293.
[62] I.M. El-Mehasseb, A.M. Ramadan, R.M. Issa, Transition Met. Chem. 31 (2006) 730 [and the references therein].